

Article

Role of Chemically Magnetized Nanofluid Flow for Energy Transition over a Porous Stretching Pipe with Heat Generation/Absorption and Its Stability

Zeeshan ^{1,†} , N. Ameer Ahammad ², Nehad Ali Shah ^{3,*} , Jae Dong Chung ³ and Attaullah ⁴ ¹ Department of Mathematics and Statistics, Bacha Khan University, Charsadda 24420, KP, Pakistan² Department of Mathematics, Faculty of Science, University of Tabuk, Tabuk 71491, Saudi Arabia³ Department of Mechanical Engineering, Sejong University, Seoul 05006, Republic of Korea⁴ Department of Mathematics, Abdul Wali Khan University, Mardan 25000, KP, Pakistan

* Correspondence: nehadali199@sejong.ac.kr

† These authors contributed equally to this work and are co-first authors.

Abstract: The laminar movement in an expanding and contracting permeable pipe or surface has recently attracted the attention of many scholars owing to its application in engineering and biological processes. The objective of the current study is to examine the influence of chemical processes on magnetized nanofluid flow over extending or shrinking permeable pipes with a heat reservoir. The flow equations are renovated into first ODEs by introducing the new variable and then numerically solved by RK4 with a shooting procedure. The effect of emerging factors on the flow features is observed using graphs and elaborated in detail. From the analysis, the temperature is raised when the heat source is increased in both cases of wall expansion or contraction but declines in the case of heat sinks. In the case of a heat source, the temperature rises as the Hartmann and Prandtl numbers are enhanced, but in the case of a heat sink, the temperature falls. In the presence of heat sinks and injections, when the thermophoresis factor is increased, the concentration of nanoparticles is increased in both wall expansion and contractions. In both situations of wall extension or contraction, along with injection, the concentration of nanoparticles is a decreasing function of Nb , while the concentration of nanoparticles is an increasing function in the case of a heat source. Additionally, for the confirmation of the RK4 code, the total average square residue error and average square residue error are also presented. For the stability analysis, the current work is compared with published work, and excellent agreement is established. The novelty of the present study is to investigate the effect of chemical reaction on magnetized nanofluid flow over extending and shrinking porous pipes with heat generation and absorption.

Keywords: RK4 and HAM; expanding/contracting pipe; heat generation/absorption; total and average square residue errors; stability analysis; nanofluid flow; chemical reaction

MSC: 76D05; 76-10



Citation: Z.; Ahammad, N.A.; Shah, N.A.; Chung, J.D.; A. Role of Chemically Magnetized Nanofluid Flow for Energy Transition over a Porous Stretching Pipe with Heat Generation/Absorption and Its Stability. *Mathematics* **2023**, *11*, 1844. <https://doi.org/10.3390/math11081844>

Academic Editor: Lihua Wang

Received: 7 February 2023

Revised: 26 February 2023

Accepted: 3 March 2023

Published: 13 April 2023



Copyright: © 2023 by the authors. Licensee MDPI, Basel, Switzerland. This article is an open access article distributed under the terms and conditions of the Creative Commons Attribution (CC BY) license (<https://creativecommons.org/licenses/by/4.0/>).

1. Introduction

The establishment of nanofluid innovation is a crucial field of research in physics, industry, mathematics, and chemical science. For the majority of applications with a practical purpose, designers and scientists work to successfully communicate sufficient knowledge of the heat transfer mechanism in nanofluids. Nanofluids are essential in a variety of applications, such as heat exchangers, freezers, hybrid-driven motors, food processing, and chips. The term “nanofluid” was originally used by Choi et al. [1]. Nanoparticles are now the subject of major scientific investigation because of their many applications in biological, optical, and electrical areas. They may be discovered in nanometals [2–7] and graphite, as well as oxides, carbides, nitrides, and metals such as copper and aluminum.

Buongiorno investigated the diffusion of heat in nanofluids (NFs) [8]. Moreover, Buongiorno [9] concluded that Brownian and thermophoresis diffusion would be important when turbulent impacts are absent. The unsteady BLF over a flowing sheet was examined by Rosca et al. [10] using Buongiorno's model. Kuznetsov et al. [11] studied the significance of bioconvection on MHD tangent hyperbolic nanofluid flow of irregular thickness across a slender elastic surface. The micropolar dusty fluid with coriolis force effects on dynamics of MHD rotating fluid when Lorentz force is significant by Lou et al. [12]. The magnetic BLF toward an extended sheet, including nanoparticles, was examined analytically by Mustafa et al. [13] using HAM. Alsaedi et al. [14] have achieved an analytical solution for the SPF when the heat source passes via a convective sheet. Chamkha et al. [15] studied the convective BLF of NFs approaching a vertical sheet. Malvandi et al. [16] discussed NFFs (nanofluid flows) employing a vertical pipe, utilizing Buongiorno's model (BM). Across a vertical tube, Akbari et al. [17] examined a fully evolved NFF. Ellahi [18] found a mathematical solution for the magnetic and changing viscosity viscous fluid within a pipe. An MHD NFF, incorporating the slip impact at the border, was seen by Uddin et al. [19] across the extended sheet. To explore the BLF traveling via a vertical stretched channel, Xu et al. [20] and Malik et al. [21] studied the BM and Casson nanofluids, respectively. The nonlinear movements of axisymmetric ternary hybrid nanofluids in a thermally radiated expanding or contracting permeable Darcy Walls with different shapes and densities using simple linear regression by Raju et al. [22]. Further examined were the Brownian and thermophoresis variables. Ramesh et al. [23] developed a flow of hybrid CNTs past a rotating sphere subjected to thermal radiation and thermophoretic particle deposition. Presently, Srinivas et al. [24] have researched the MHD flow of NFs in a permeability-expanding pipe. Hedayati et al. [25] very recently investigated titania water-related nanofluids across a ferromagnetic vertical cylindrical conduit. Malvandi et al. [26] also looked at an alumina water-based nanofluid across a vertical channel using the Lorentz force effect. Chemical engineering, metallurgy, radioactive nuclear safety, photovoltaic collectors, and other nanotechnology and scientific fields have been shown to significantly impact heat transport [27–29]. The impact of chemical efficiency on blood flow using Walter's B model across a tapered artery was taken into consideration by Nadeem et al. [30]. Hayat et al.'s [31] examined Maxwell fluids' biochemical processes. Abdul et al. [32] examined the chemical reactions taking place over a stretchy sheet that was saturated with nanofluids, utilizing the BLF. Kameswaran et al. [33] investigated uniform and heterogeneous chemical reactions across a porous stretching surface. The MHD laminar BLF, with a slip impact over a stretched permeable surface with chemical reactions, was numerically explored by Uddin et al. [34]. For free convection flow (FCF) across a horizontal surface containing nanofluids, an analytical solution was discovered [35]. Recently, Srinivas et al. [36] examined a viscoelastic fluid across a chemically stretched pipe. Uddin et al. [37] investigated the MHD FCBLF with NF chemical reactivity via a vertical surface. The laminar movement in an escalating or shrinking permeable pipe or surface has recently attracted the curiosity of many scholars owing to its application in engineering and biological developments, for example, in the transportation of natural fluids through stretching vessels, the synchronous rhythm of absorbent diaphragms, the respiratory system, and the deterioration of the red-hot sheet in rock-solid engines [38–40]. The thermal flux and heat transfer have been studied by many researchers (see [41–45]). The unsteady fluid flow over semi-infinite stretching pipes with a heat source was examined by Boutros et al. [46] via the Lie group approach. Zeeshan [47] investigated the energy activation analysis for Maxwell fluid comprising molybdenum disulfide and graphene nanoparticles in engine-based fluid, enclosing the effect of isothermal wall temperature. Rasheed et al. [48] scrutinized the movement of micropolar fluid over an extended surface with thermal radiation influence. Zeeshan et al. [49] obtained the numerical solution for entropy generation by scrutinizing the second-order nanofluid's thin film flow with error and stability analyses. Recently, the influence of heat and transfer analyses of nanofluids over a horizontal surface with thermal and magnetic field effects was investigated by Zeeshan et al. [50]. Raza et al. [51] investigated the movement of MHD Casson liquid over

a porous sheet with extended and stationary walls. Khan et al. [52] obtained the exact solution of a Casson model movement situated with dust particles through a stretching surface enclosing the Lorentz forces. Similarly, Chabani et al. [53] numerically investigated a magnetized hybrid nanofluid over a porous trapezoidal inclusion.

The above study reveals that no effort towards the influence of chemical processes on magnetohydrodynamic NFFs over a stretchable permeable pipe enclosing the effect of a heat reservoir has been scrutinized so far. Such deliberation has a significant value in science and engineering study, including chips, refrigerators, hybrid powered motors, food improvement, heat exchangers, and so on. Keeping the overhead observations in view, the purpose of the recent study is to observe the inspiration of chemical processes on magnetized nanofluid flows over extending or shrinking permeable pipes with a heat reservoir. The flow characteristics are renovated into first ODEs by introducing the new variable and then numerically elucidated using the Runge–Kutta fourth-order method with a shooting technique [54]. The effect of emerging parameters on the flow features is observed using graphs and elaborated in detail. Additionally, the confirmation of RK4 is compared with HAM. For the stability analysis, the current work is likened to the available literature, and exceptional correlation is established.

2. Formulation of the Problem

The unsteady NFF of an electrically conducting fluid in a semi-infinite length over an equally porous pipe is considered. The pipe has a radius, $\hat{a}(t)$. The wall is the function of time t that is expanding and shrinking with time. Figure 1 demonstrates the geometry of the present problem, in which its origin is taken at the center of the pipe, where z -axis is parallel to the wall and r is normal to the wall.

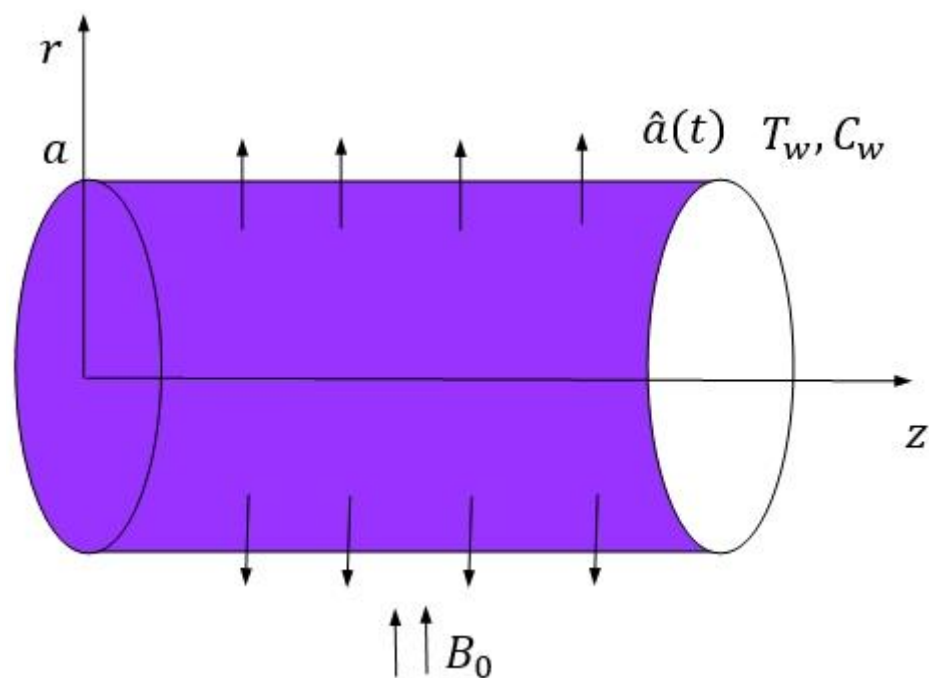


Figure 1. Geometrical presentation of the problem.

The central equations are under these presumptions [16–22]:

$$\frac{\partial u}{\partial z} + \frac{\partial v}{\partial r} + \frac{v}{r} = 0 \tag{1}$$

$$\frac{\partial u}{\partial t} + u \frac{\partial u}{\partial z} + v \frac{\partial u}{\partial r} = -\frac{1}{\rho_f} \frac{\partial p}{\partial z} + \nu \left[\frac{\partial^2 u}{\partial r^2} + \frac{1}{r} \frac{\partial u}{\partial r} + \frac{\partial^2 u}{\partial z^2} \right] - \frac{\sigma B_0^2}{\rho_f} u \tag{2}$$

$$\frac{\partial v}{\partial t} + v \frac{\partial v}{\partial z} + v \frac{\partial v}{\partial r} = -\frac{1}{\rho_f} \frac{\partial p}{\partial r} + v \left[\frac{\partial^2 v}{\partial r^2} + \frac{1}{r} \frac{\partial v}{\partial r} + \frac{\partial^2 v}{\partial z^2} - \frac{v}{r^2} \right] \tag{3}$$

$$\frac{\partial T}{\partial t} + u \frac{\partial T}{\partial z} + v \frac{\partial T}{\partial r} = \beta \left[\frac{\partial^2 T}{\partial r^2} + \frac{1}{r} \frac{\partial T}{\partial r} + \frac{\partial^2 T}{\partial z^2} \right] + \tau \left[D_B \left(\frac{\partial C}{\partial r} \frac{\partial T}{\partial r} + \frac{\partial C}{\partial z} \frac{\partial T}{\partial z} \right) + \frac{D_T}{T_m} \left\{ \left(\frac{\partial T}{\partial r} \right)^2 + \left(\frac{\partial T}{\partial z} \right)^2 \right\} \right] + \frac{Q_0}{(\rho C_p)_f} (T - T_0) \tag{4}$$

$$\frac{\partial C}{\partial t} + u \frac{\partial C}{\partial z} + v \frac{\partial C}{\partial r} = D_B \left(\frac{\partial^2 C}{\partial r^2} + \frac{1}{r} \frac{\partial C}{\partial r} + \frac{\partial^2 C}{\partial z^2} \right) + \frac{D_T}{T_m} \left\{ \frac{\partial^2 T}{\partial r^2} + \frac{1}{r} \frac{\partial T}{\partial r} + \frac{\partial^2 T}{\partial z^2} \right\} - kC \tag{5}$$

where z and r represent directions, and u, v represent the components of the velocity. The fluid density is ρ_f , thermal diffusivity is β , time is t , kinematic viscosity is ν , dimensional pressure is p , magnetic field strength is B_0 , and electrical conductivity is σ , C_p represents the specific heat, the average (mean) temperature is T_m , Brownian and thermophoretic diffusion coefficients are D_B and D_T , respectively, and T and C stand for temperature and nanoparticle concentration, respectively; $\tau = \frac{(\rho C_p)_p}{(\rho C_p)_f}$, while k represents the first-order chemical reaction rate ($k < 0$ for a generative reaction (GR), $k > 0$ for a destructive reaction (DR), and $k = 0$ for no reaction).

The pertinent boundary constraints are

$$u = 0, \quad v = -v_w = -A\hat{a}, \quad T = T_w, \quad C = C_w \quad r = a(t) \tag{6}$$

$$\frac{\partial u}{\partial r} = 0, \quad v = 0, \quad \frac{\partial T}{\partial r} = 0, \quad \frac{\partial C}{\partial r} = 0 \quad \text{at } r = 0 \tag{7}$$

$$u = 0, \quad v = 0 \quad \text{at } z = 0. \tag{8}$$

The wall permeability is represented by the A (injection/suction coefficient) in Equation (6), where T_w, C_w are the wall's temperature and concentration, respectively.

Add a stream function that meets the continuity requirement in Equation (1)

$$\psi = vzf(\eta, t) \tag{9}$$

where the dimensionless radial location is represented by $\eta = \frac{r}{a}$. You can write the radial and axial velocity components as

$$\begin{aligned} u &= \frac{1}{r} \frac{\partial \psi}{\partial r} = \frac{vzf_\eta(\eta, t)}{a^2\eta} \\ v &= \frac{1}{r} \frac{\partial \psi}{\partial z} = -\frac{vf_\eta(\eta, t)}{a\eta} \end{aligned} \tag{10}$$

One may obtain this by replacing Equation (10) with Equations (2) and (3) after removing pressure.

$$\begin{aligned} \eta^2 f_{\eta\eta\eta\eta} + (\alpha\eta^3 - 2\eta) f_{\eta\eta\eta} + (\alpha\eta^2 + 3) f_{\eta\eta} - \left(\alpha\eta + \frac{3}{\eta} \right) f_\eta + f_\eta^2 - \eta f_\eta f_{\eta\eta} + \eta f f_{\eta\eta\eta} \\ - 3f f_{\eta\eta} + \frac{3}{\eta} f f_\eta - M^2 (\eta^2 f_{\eta\eta} - \eta f_\eta) - \frac{a^2}{\nu} \left(\frac{f_\eta}{\eta} \right)_{\eta t} \eta^3 = 0. \end{aligned} \tag{11}$$

where $M = \frac{\sqrt{\sigma B_0 a}}{\sqrt{\mu}}$ is the Hartmann number (HN), and μ is the viscosity. The non-dimensional wall dilation rate is defined as $\alpha = \frac{a\hat{a}}{\nu}$, being positive for extension and negative for shrinkage. The associated boundary constraints from Equations (6) through (8) convert into

$$\begin{aligned} f(0, t) = 0, \quad f(1, t) = R, \quad f_\eta(1, t) = 0, \\ \lim_{\eta \rightarrow 0} \frac{\partial}{\partial \eta} \left(\frac{1}{\eta} \frac{\partial f(\eta, t)}{\partial \eta} \right) = 0 \end{aligned} \tag{12}$$

$R = \frac{av_w}{\nu} = A\alpha$ defines the permeation Reynolds number (PRN) as follows: R is positive for inoculation but negative for suction, as you can see. By separately applying the transformations outlined by Si et al. [9] and Uchida and Aoki [7], a comparable solution

with regard to both time and space may be created. It follows that $\left(\frac{f_\eta}{\eta}\right)_{\eta t} = 0$ for constant α and $f = f(\eta)$. To fulfil this requirement, the expansion ratio's α value must be determined by the beginning value.

$$\alpha = \frac{a\hat{a}}{v} = \frac{a_0\hat{a}_0}{v} = constant \quad \text{or} \quad \frac{\hat{a}_0}{\hat{a}} = \frac{a}{a_0} \tag{13}$$

where a_0, \hat{a}_0 define the initial radius and growth rate correspondingly. By integrating Equation (13) with regard to time, the temporal similarity transformation may be accomplished. The outcome is

$$\frac{a}{a_0} = \sqrt{1 + 2v\alpha t a_0^{-2}}. \tag{14}$$

It is demonstrated that the injection coefficient A is constant since $v_w = A\hat{a}$ may be used to calculate an equation for the injection velocity. It is evident from Equations (13) and (14),

$$\frac{\hat{a}_0}{\hat{a}} = \frac{v_w(0)}{v_w(t)} = \sqrt{1 + 2v\alpha t a_0^{-2}}. \tag{15}$$

$$\eta^3 f'''' + \alpha(\eta^4 f''' + \eta^3 f'' - \eta^2 f) - 2\eta^2 f''' + 3\eta f'' - 3f' + \eta f'^2 - 3\eta f f'' + 3f f' + 3\eta^2 f f''' - \eta^2 f' f'' - M^2(\eta^3 f'' - \eta^2 f') = 0. \tag{16}$$

These boundary constraints are

$$f(0, t) = 0, \quad f'(1, t) = 0, \quad f(1) = R, \quad \lim_{\eta \rightarrow 0} \left(\frac{f'}{\eta}\right)' = 0. \tag{17}$$

One can normalize Equations (10), (16), and (17) by inputting Equation (18) and ignoring the “*”; we get

$$\psi^* = \frac{\psi}{a\hat{a}}, \quad u^* = \frac{u}{\hat{a}}, \quad v^* = \frac{v}{\hat{a}}, \quad z^* = \frac{z}{a}, \quad f^* = \frac{f}{R}. \tag{18}$$

$$\eta^3 f'''' + \alpha(\eta^4 f''' + \eta^3 f'' - \eta^2 f) - 2\eta^2 f''' + 3\eta f'' - 3f' + \eta R f'^2 - 3\eta R f f'' + 3R f f' + 3\eta^2 R f f''' - \eta^2 f' f'' - M^2(\eta^3 f'' - \eta^2 f') = 0. \tag{19}$$

$$f(0) = 0, \quad f'(0) = 0, \quad f(1) = 1, \quad \lim_{\eta \rightarrow 0} \left(\frac{f'}{\eta}\right)' = 0. \tag{20}$$

It should be noticed that Equation (19) describes the situation that Majdalani et al. [13] have outlined when $\alpha = 0$ and $M = 0$ exist. The relationship between the temperature and the concentration in the pipe is as follows:

$$T = T_0 + (T_w - T_0)\theta(\eta), \quad C = C_0 + (C_w - C_0)\phi(\eta), \tag{21}$$

where T_0 and C_0 are the reference temperatures and concentrations of nanoparticles at the center. From Equation (21), the dimensionless temperature and nanoparticle concentration are

$$\theta = \frac{T - T_0}{T_w - T_0}, \quad \phi = \frac{C - C_0}{C_w - C_0}. \tag{22}$$

Equation (21) is substituted into Equations (4) and (5) to get

$$\eta\theta'' + \alpha Pr\eta^2\theta' + RPrf\theta' + Nb\eta\theta'\phi' + Nt\eta\theta'^2 + \theta' + QPr\eta\theta = 0 \tag{23}$$

$$\eta\phi'' + \alpha PLePr\eta^2\phi' + RLePrf\phi' + \eta\frac{Nt}{Nb}\theta'' + \frac{Nt}{Nb}\theta' + \phi' + \gamma LePr\eta\phi - LePrK_1\eta = 0 \tag{24}$$

with the boundary constraints

$$\theta'(0) = 0, \theta(1) = 1, \phi'(0) = 0, \phi(1) = 1. \tag{25}$$

Here $Pr = \frac{\nu}{\beta}$, $Nb = \frac{\tau D_B(C_w - C_0)}{\beta}$, $Nt = \frac{\tau D_T(T_w - T_0)}{T_m \beta}$, $Le = \frac{\beta}{D_B}$, $Q = \frac{Q_0 a^2}{(\rho C_p)_f \nu}$, and $\gamma = \frac{k_1 a^2}{\nu}$ represent the Prandtl number, Brownian motion, the thermophoresis factor, the Lewis number, the sink/heat source (i.e., $Q < 0$ for a heat sink and $Q > 0$ for a heat source), and the chemical reaction factor, respectively, and $K_1 = \frac{k C_0 a^2}{\nu(C_w - C_0)}$.

3. Numerical Procedure and Convergence

The scheme of Equations (23)–(25) is solved by RK4. For this solution, Equations (23) and (25) are first transformed to the conventional first ODEs by introducing new variables and then solved numerically by keeping step size $\Delta\eta = 0.01$ and obtaining the convergence criteria up to 10^{-5} . For endorsement of the consequences, the HAM is also functional, and brilliant settlement is originated as shown in (Figure 2). The procedure of the numerical method is given in (Figure 3). Detailed information on this method is given in [31]. Additionally, the current effort is likened to the previous and brilliant settlement originated, as revealed in Tables 1 and 2.

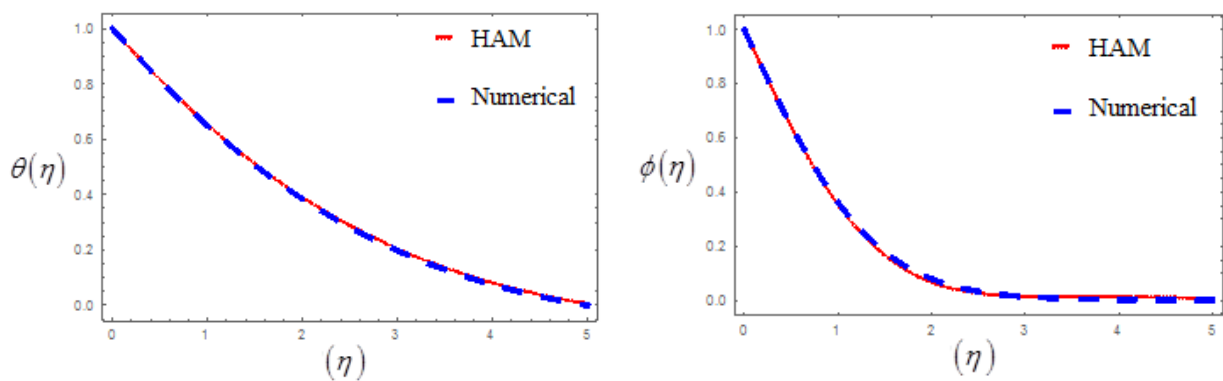


Figure 2. Assessment of RK4 and HAM for $\theta(\eta)$ and $\phi(\eta)$.

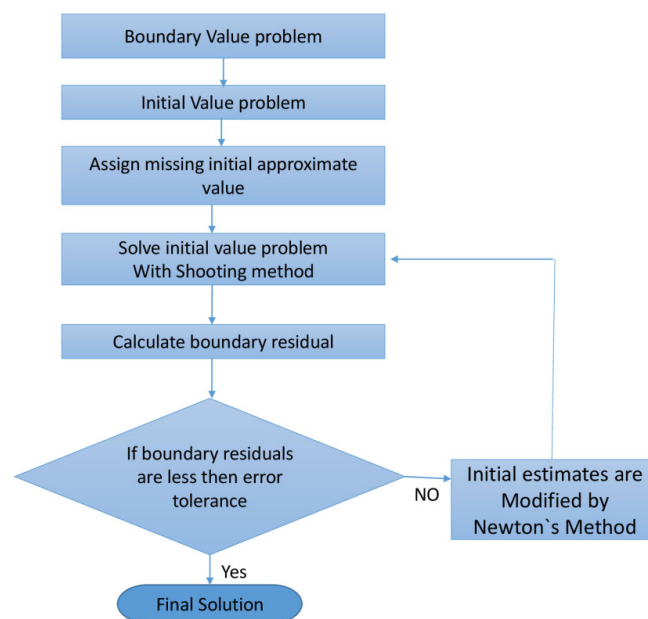


Figure 3. Flow chart of the numerical algorithm.

Table 1. Variation of radial velocity in the suction case for the viscous fluid; $M = 0, R = -50$.

α	η	Srinivas et al. [49]	25th-Order Approximation
3	0.92763	-1.1398871	-1.147523
2	0.99429	-1.166290	-1.166291
0	0.87134	-1.179535	-1.179537
-3	0.87134	-1.182623	-1.182623
-2	0.87134	-1.187371	-1.187371

Table 2. Variation of radial velocity in the suction case for the viscous fluid; $M = 0, R = -100$.

α	η	Srinivas et al. [49]	25th-Order Approximation
3	0.97289	-1.173991	-1.176380
2	0.97134	-1.176393	-1.178475
0	0.87134	-1.177947	-1.179692
-3	0.87134	-1.178881	-1.178881
-2	0.87134	-1.179290	-1.179290

4. Stability Analysis

The numerical solution has been obtained for the nonlinear differential equation for the temperature and concentration profiles. For the stability analysis of the mathematical problem, the present work is compared with the published work. Tables 1 and 2 show that for up to 25 orders of approximation, the comparison of the present work and the published work reported by Srinivas et al. [49] shows excellent agreement.

5. Error Explanation

For most linear first-order differential equations, the RK4 approach yields solutions that are typically trustworthy. Significant errors are quite improbable, but that is because the conclusions are based on computer sampling and error calculations. Examining results using a solution that is derived with working precision that is higher than the Machine Precise standard is often helpful. The RK4 method is used to compute the answer to the issue with the usual work precision, and the same method is used to calculate the error with working precision-22. As errors are often rather small, it is useful to evaluate them on a logarithmic scale. The following graphs show the incorrect solutions we generated for the various physical parameters utilized in the model.

We initially conducted an error evaluation to check the validity of the process before establishing any physical predictions. This is the purpose for the creation of Figures 4–7. The minimum mistake 10^{-30} of the RK4 program is corrected during the solution by using the ND-Solve Mathematica package to reduce the overall average squared residual error (ASRE). We initially modified the thermal radiation factor R_d and fixed $Gr = Gm = 1, Pr = 5, Q = 0.3, Ec = 0.4, Sc = 0.2,$ and $Sc = 1.5$ to observe the error for numerous orders of approximation. The greatest ASRE at various interpolation orders is shown in Figures 4 and 5.

In Figure 4, it is seen that for $\alpha = -1$, total ASRE and ASRE are decreasing as the order of approximation increases. Additionally, for $\alpha = 0.1$, the error is streakily decreasing compared to the cases for $\alpha = 0.8$, as exposed in Figure 5. By changing the magnetic parameter of $M = 0$ and $M = 0.1$, setting $Gr = Grm = 2, Pr = 3, Q = 0.5, Ec = 0.1, Prm = 0.5,$ and $Sc = 0.7$, similarly distinct plots are given in Figures 6 and 7, respectively. Averaged squared residual errors and total averaged squared residual errors both decrease for $\alpha = 0.1, 0.8$ and $M = 0, 0.1$ as the order of approximation increases. It is also observed that for $\alpha = M = 0.1$ the error streakily reduces, as related to the cases for $\alpha = 0.8$ and $M = 0.1$ and shown in Figures 6 and 7.

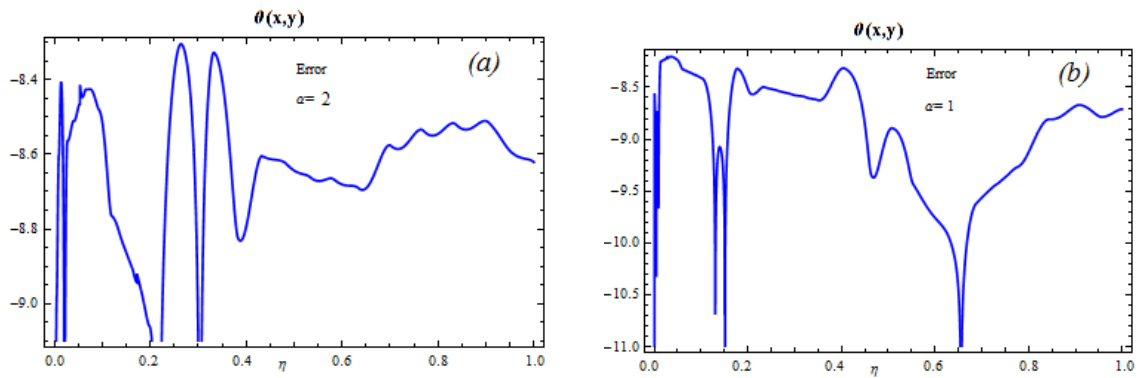


Figure 4. Temperature error analysis for physical parameters (a) $\alpha = 2$ and (b) $\alpha = 1$.

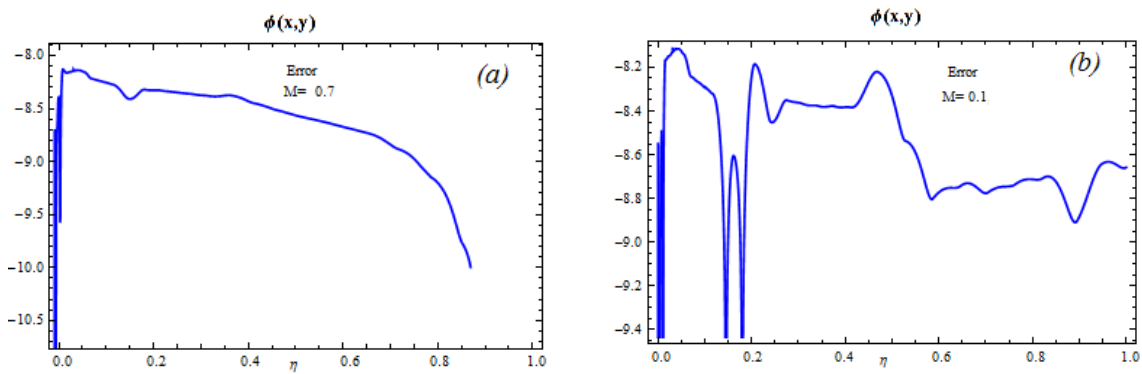


Figure 5. Concentration error analysis for physical parameters (a) $M = 0.7$ and (b) $M = 0.1$.

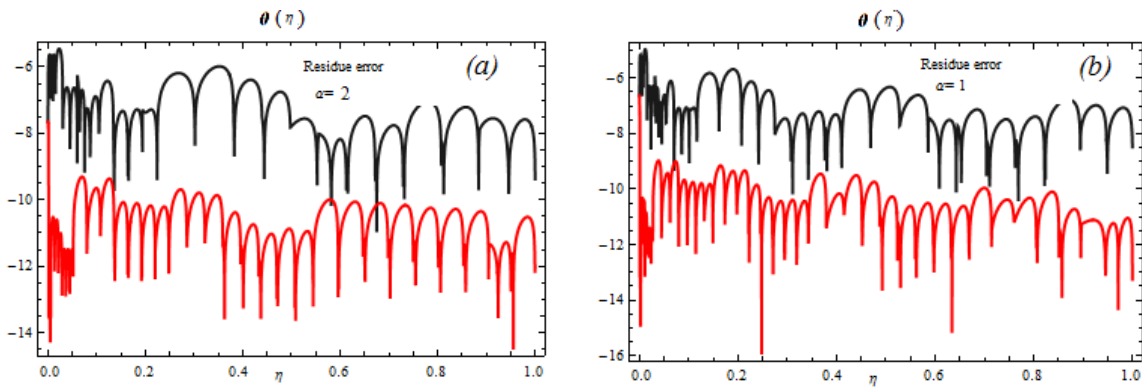


Figure 6. Residue error for temperature for physical parameters (a) $\alpha = 2$ and (b) $\alpha = 1$.

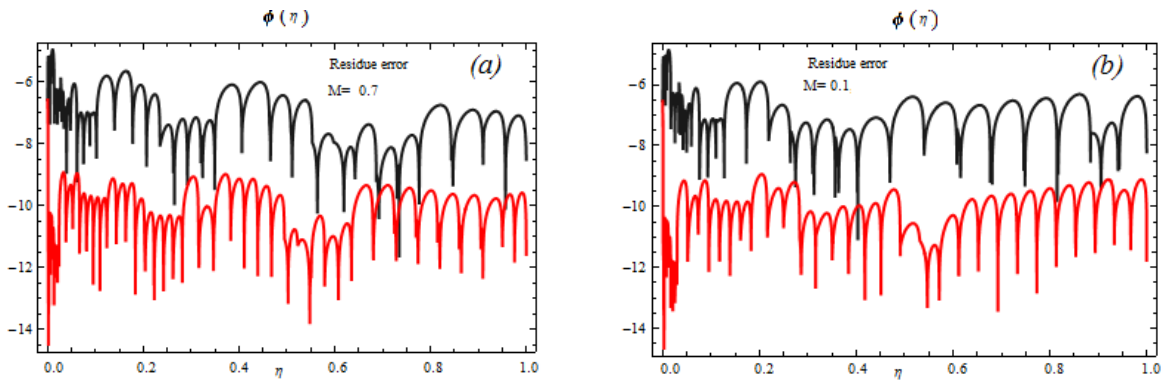


Figure 7. Residue error for concentration for physical parameters (a) $M = 0.7$ and (b) $M = 0.1$.

6. Analysis and Discussion

This section examines the consequence of several physical factors on the flow characteristics, such as the Nusselt number, Sherwood number, non-dimensional temperature, and nanoparticle concentration. Figures 8–21 provide a graphic representation of the outcomes against $0 \leq \eta \leq 1$. The effect of numerous factors such as the thermophoresis factor Nt , the heat source/sink factor Q , the wall extension ratio, the Hartmann number M , the Prandtl number Pr , the Brownian motion factor Nb and the permeation parameter R , the Lewis number Le , and the chemical reaction parameter are discussed in detail. For a better understanding of the physical interpretation of the physical parameters, we chose $Pr = 6$, $Nb = Nt = 0.3$, $Le = 0.6$, $Q = 0.3$, $\gamma = 0.5$, and $M = 0.1$. It should be emphasized that the variables Nb and Nt describe the magnitudes of Brownian movement and thermophoresis impacts, respectively. The greater quantities of Nb and Nt have stronger consequences. Hence, Nb and Nt can have any value between $0 \leq Nb < \infty$. Figures 8a, 9, 10, 11, 12, 13 and 14b illustrate the influence of various parameters, including the sink parameter or heat source, the Brownian motion factor, the thermophoresis factor, the ratio of the wall extension, the Hartmann number, the permeation Reynolds factor, and the Prandtl number, on the temperature field. The effects of the Brownian factor on the temperature field for both situations of injection, including wall extension and shrinking, are exposed in Figure 8a,b. It is noted that the temperature rises in injection with wall expansion and contraction by enhancing Nb for $Q < 0$. In the injection situation, the concentration of nanoparticles migrates from the wall to the liquid, which causes a considerable rise in the temperature field. For $Q > 0$, the opposite behavior is observed. Figure 9a,b illustrates how the heat source/sink parameter affects the temperature in the circumstances of both injections, combined with wall shrinking and expansion. It is observed that the heat source raises the temperature in both situations of injection, along with wall contraction and moderation, but a heat sink lowers it. The influence of the thermophoresis factor on energy is depicted in Figure 10a,b for the injection situation, along with wall extension and contraction. For a certain rise in Nt , it is observed that the temperature is enhanced. Figure 11a,b show the relationship between temperature and the wall expansion ratio. In the event of wall extension, regardless of injection or suction, if it increases α in the presence of a heat generation (i.e., $Q < 0$), then the temperature increases; if $|\alpha|$ grows in the case of wall shrinkage, then the temperature decreases. However, in the event of a heat source, the behavior is the opposite (for $Q > 0$). The influence of the Hartmann number (HN) on the temperature field is shown in Figure 12a,b. It has been noted that nanofluids exhibit similar properties to ordinary fluids in terms of temperature regarding the Hartmann number. As Ha grows, the temperature rises in the existence of a heat source for both the expansion and contraction of the wall. In a heat sink, the reverse observation is observed. Figure 13a,b explore the effect of the Prandtl number on the temperature. It is essential to remember that the Prandtl number describes liquid metals and oils. Larger values of Pr are associated with high viscosity oils, whereas smaller values of Pr define liquid metals with low viscosity and thermal conductivity. Here, $Pr = 7114$, 4, and 21 corresponds to water, water at 4 °C, and human blood, individually. It is clear that in both scenarios of wall expansion and contraction associated with inoculation, the temperature falls as Pr grows (i.e., rising thermal diffusivity) in the existence of a heat sink, but it improves in the context of a heat source. The relationship between the permeation Reynolds number and the temperature is seen in Figure 14a,b. It has been found that the boundary layer thickness reduces with increasing injection, and as a consequence, the temperature declines in both scenarios of injection, together with wall extension and contraction. The reverse effect is observed in the case of suction, along with wall extension and contraction.

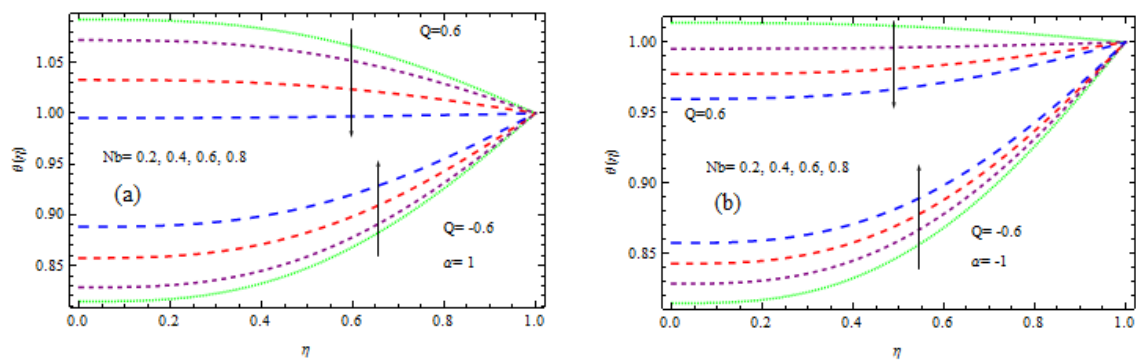


Figure 8. (a,b) Influence of Brownian factor on temperature.

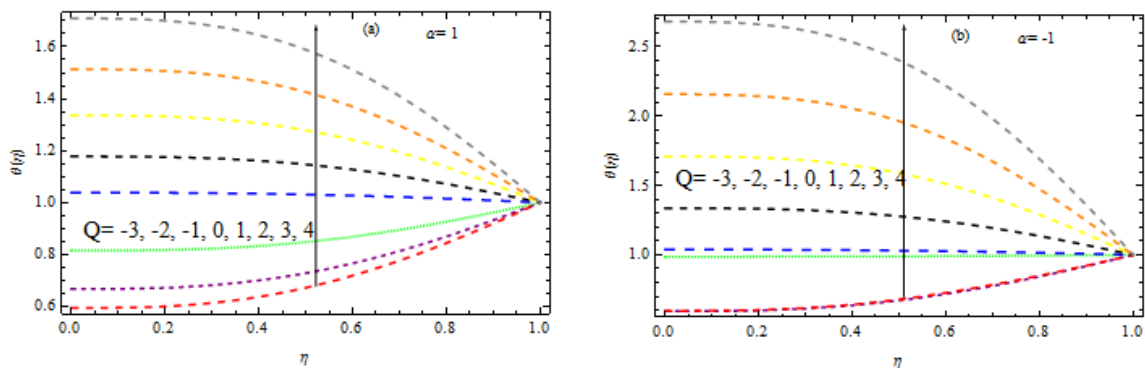


Figure 9. (a,b) Influence of heat source factor on temperature.

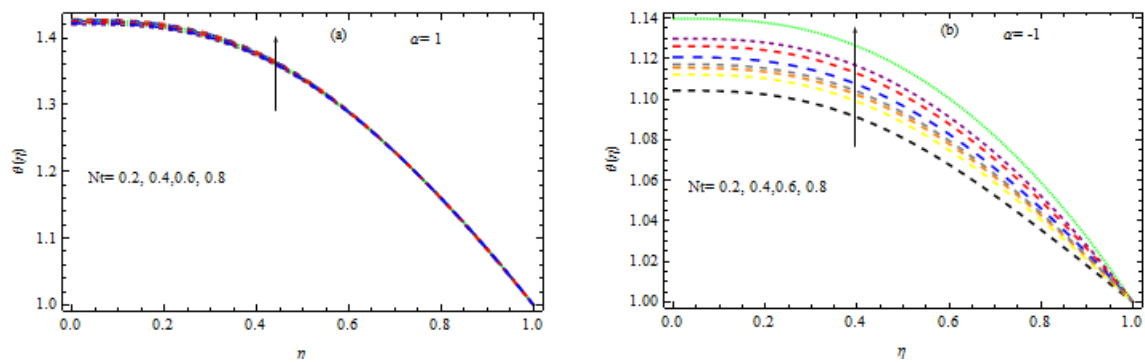


Figure 10. (a,b) Influence of Nt on temperature.

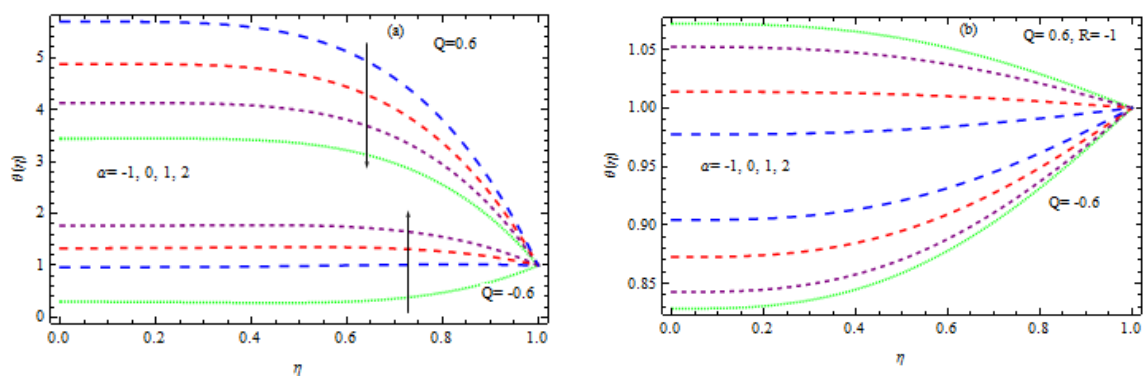


Figure 11. (a,b) Influence of wall α on temperature.

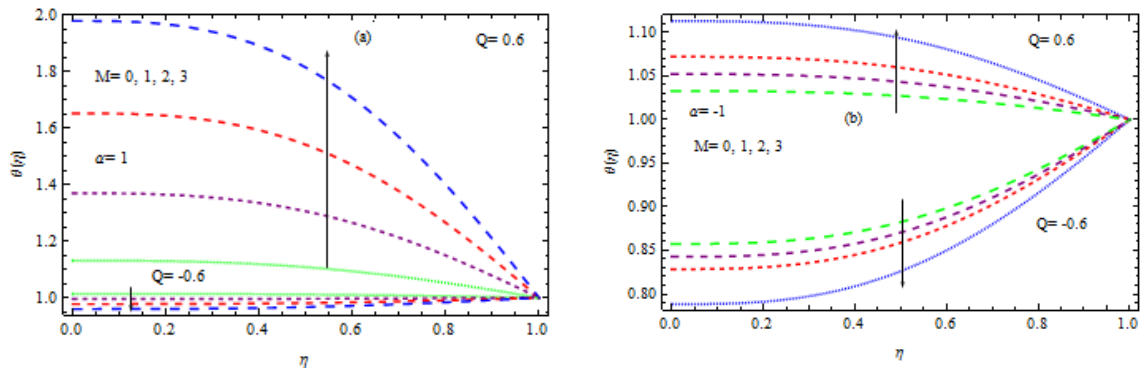


Figure 12. (a,b) Influence of M on temperature.

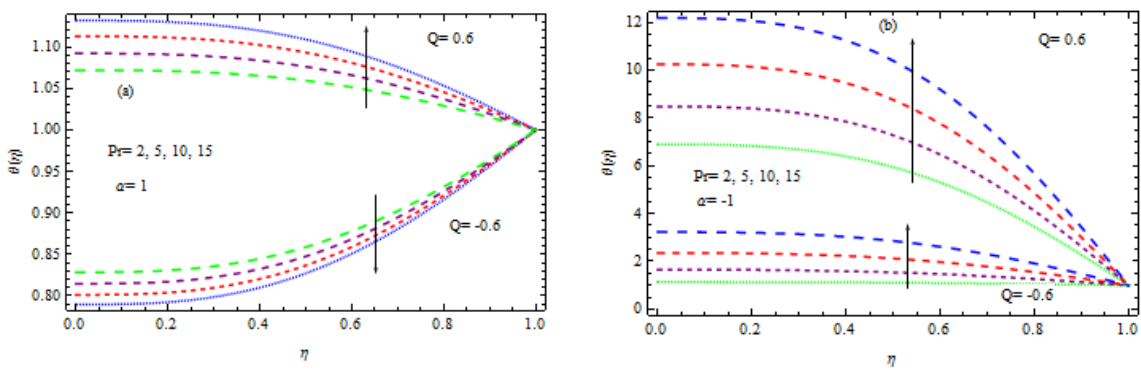


Figure 13. (a,b) Influence of Pr on temperature.

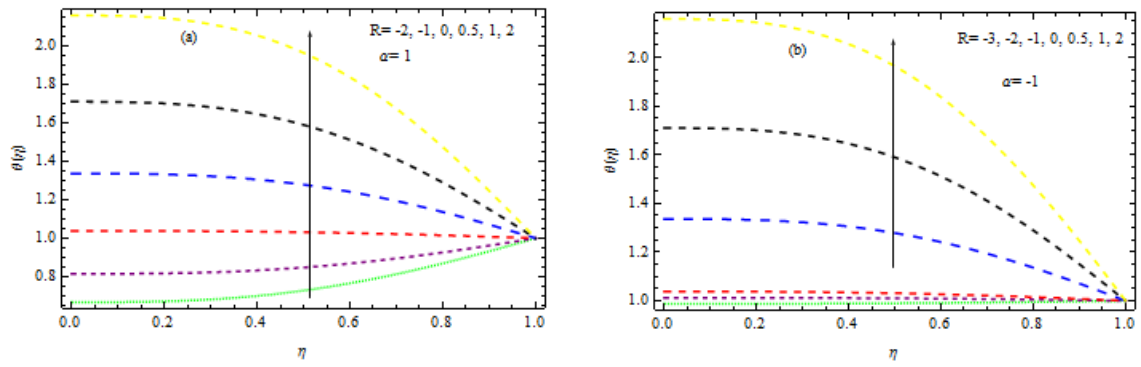


Figure 14. (a,b) Influence of R on temperature.

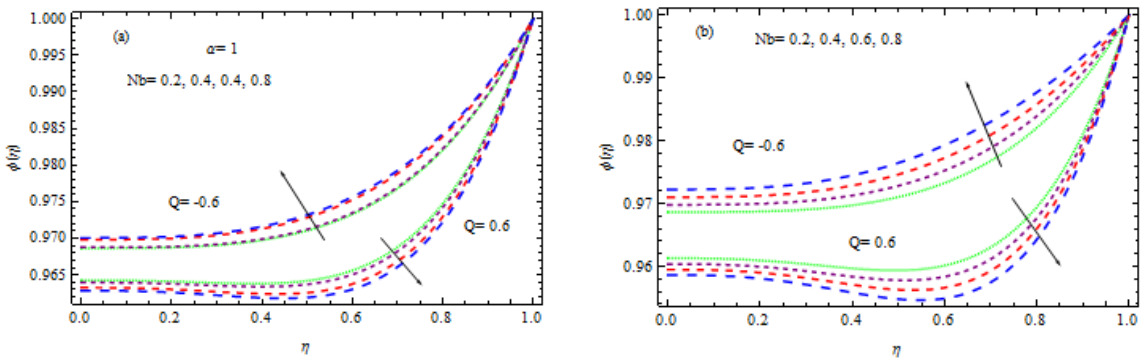


Figure 15. (a,b) Influence of Nb on temperature.

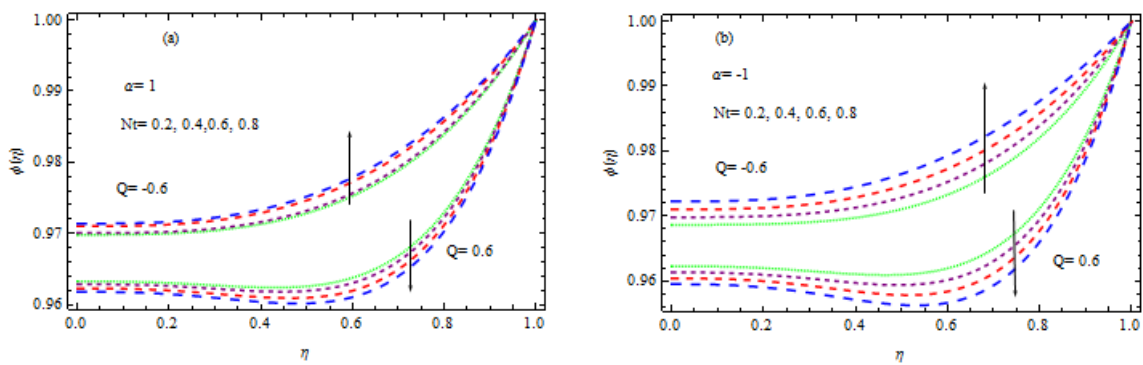


Figure 16. (a,b) Influence of Nt on temperature.

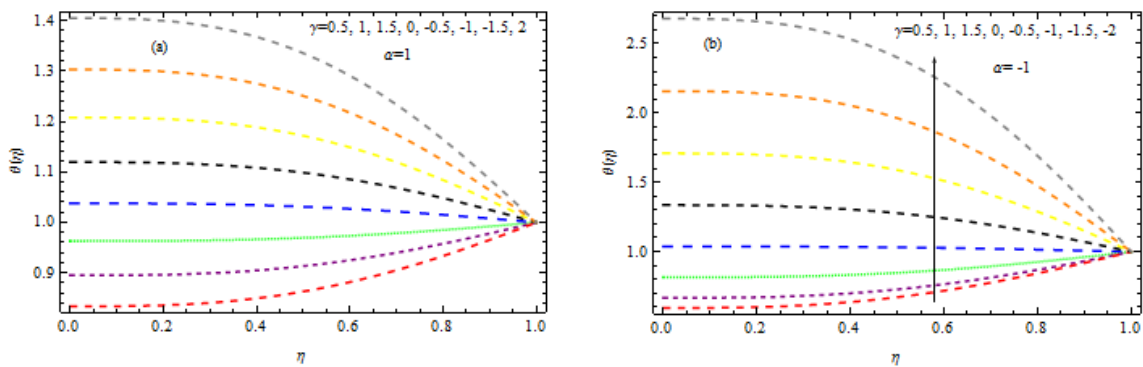


Figure 17. (a,b) Influence of γ on temperature.

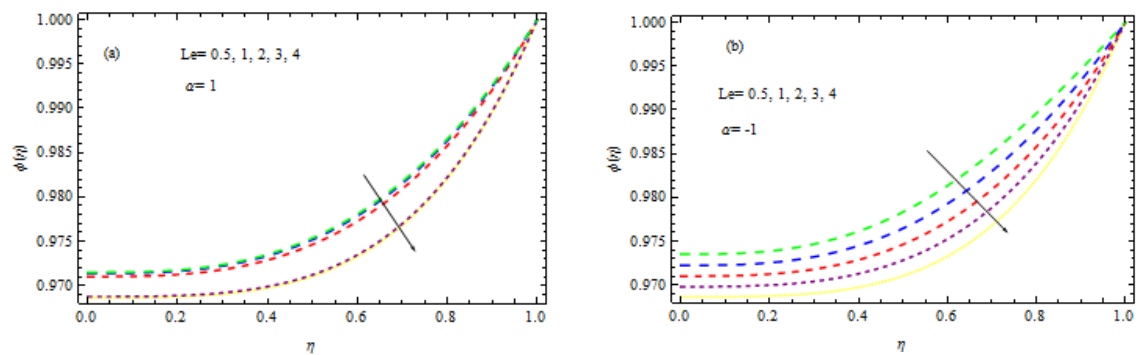


Figure 18. (a,b) Influence of Le on concentration.

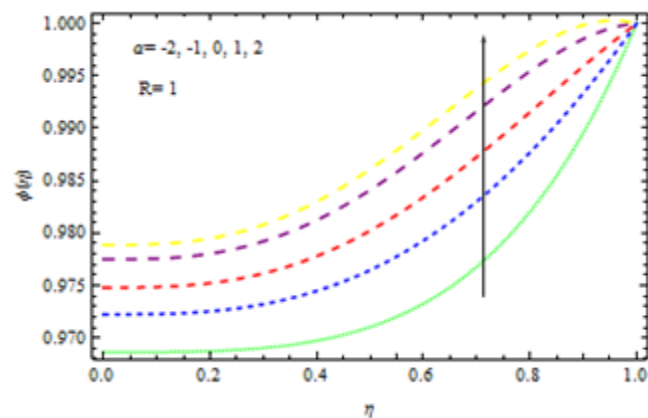


Figure 19. Influence of α on concentration.

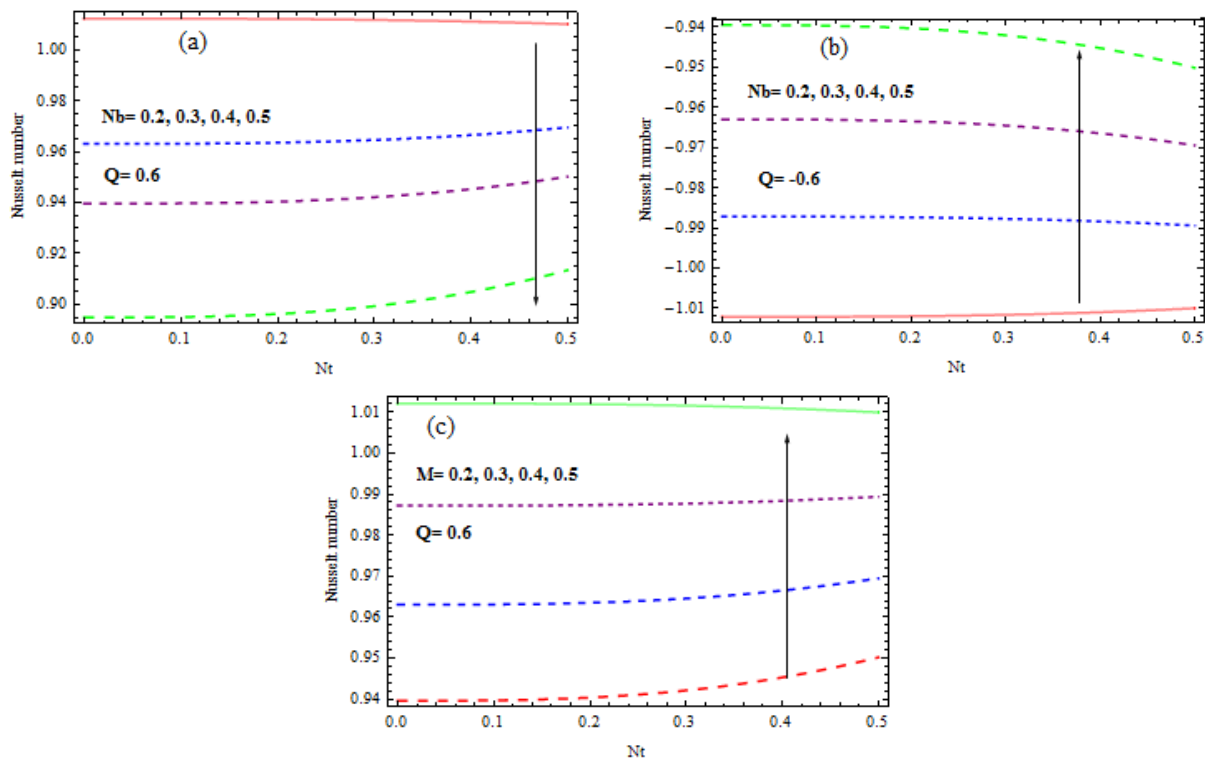


Figure 20. (a–c) Variation of Nusselt number for (a) Nb when $Q = 0.6$, (b) Nb when $Q = -0.6$, (c) M .

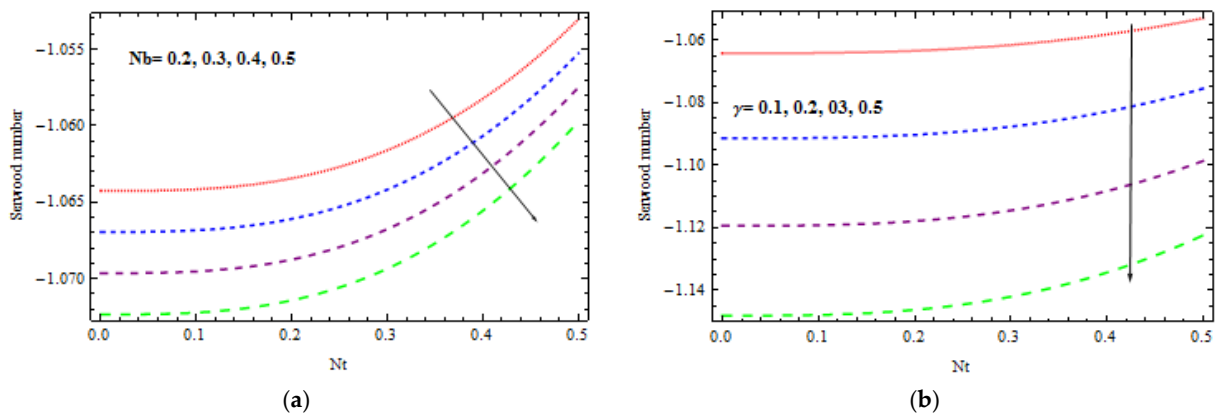


Figure 21. Variation of Sherwood number by (a) Nb , (b) γ .

Figure 15a,b, Figures 16–18 show the influence of the Lewis number, the wall expansion ratio, thermophoresis, Brownian motion, and the chemical factor on the concentration of nanoparticles. Figure 15a,b demonstrate that the concentration field declines with the growing amount of Nb in the occurrence of a heat sink, but the opposite trend is observed in the existence of heat generation and destruction for wall extension and shrinkage. The consequence of the thermophoresis factor on the concentration of nanoparticles is shown in Figure 16a,b. It is evident that for both developments of wall extension and shrinkage with injection, nanoparticle concentration is increased with increasing Nt in the existence of a heat sink. From a physical standpoint, a larger mass flux is produced by a rise in the thermophoresis parameter due to the temperature difference; as a consequence, the concentration enhances. In the manifestation of a heat source, the reverse behavior is examined in the same figure. Figure 17a,b exhibit the influence of a chemical factor, γ , on the concentration field, where the parameter is negative for a generative reaction and positive for a destructive reaction. It is noted that for an increment in γ , there is a drop

in nanoparticle concentration in the case of the destructive chemical process parameter ($\gamma > 0$). Additionally, in the event of a generative chemical process ($\gamma < 0$), the behavior is the opposite. Figure 18a,b show how the Lewis quantity Le effects ϕ . It is obvious that the function ϕ is a shrinking function of Le . When the values of the Lewis number are increased, the concentration of mass transfer is increased, which lowers nanoparticle concentration. The effect of the wall extension ratio α on ϕ is seen in Figure 19. When α increases, the nanoparticle concentration enhances for wall expansion in the occurrence of injection, although for the situation of wall contraction, it decreases as $|\alpha|$ increases.

Figure 20a–c shows the influence of the Brownian and thermophoresis factors on the Nusselt number Nu against Nt . The Nu at the pipe wall is found to be an increasing function of Nt . It is evident from Figure 20a that Nu rises when Nb rises near the wall for $Q < 0$ but falls in situation $Q > 0$ (Figure 20b). It is also analyzed from Figure 20c that Nu rises for a given rise in M at the surface of the wall. Figure 21a,b are plotted to check the inspiration of the thermophoresis and the Brownian factors versus the Sherwood number Sh . It is obvious that the Sh rises as Nt at the surface of the wall increases. Figure 21a witnesses that that Sh reduces as Nb enhances at the wall. Figure 21b shows that Sh declines for a specified growth in γ near the wall.

7. Key Notes

In this study, we investigate the influence of chemical reactions and heat reservoirs on MHD nanofluid flow in a porous expanding or contracting pipe. The characteristics equation of the flow cylinder coordinates is transformed to an ordinary differential equation and converted by using suitable transformation and then solved numerically by using the RK4 method. For the stability analysis, the present work is compared with the previous work. For the confirmation of the mathematical modeling, the error estimation and the residue error are also calculated, and it is found that the error is too small, which validates our solution. The novelty of the present study is to investigate the effect of chemical reactions on magnetized nanofluid flow over an extending and shrinking porous pipe with heat generation and absorption; in limiting cases, the present work is compared with the published work, and outstanding agreement is found.

The following summarizes the key conclusions:

1. It is observed that for both situations of wall extension or contraction with injection, the temperature is the increasing function of the thermophoresis and Brownian motion factors.
2. It is analyzed that the temperature is raised when the heat source is increased in both cases of wall expansion or contraction but declines in the case of a heat sink.
3. In the case of a heat source, the temperature rises as the Hartmann and Prandtl numbers are enhanced, but in the case of a heat sink, the temperature falls.
4. In the presence of heat sinks and injections when the thermophoresis factor is increased, the concentration of nanoparticles is increased in both wall expansion and contraction.
5. In both situations of wall expansion or contraction, along with injection, the concentration of nanoparticles is a decreasing function of Nb , while the concentration of nanoparticles is an increasing function in the case of a heat source.
6. It is also observed that ϕ is increased for $\gamma < 0$ and decreased for $\gamma > 0$.

Author Contributions: Conceptualization, Z., N.A.S. and J.D.C.; Methodology, Z., J.D.C. and A.; Software, N.A.A.; Validation, N.A.A. and N.A.S.; Formal analysis, Z., J.D.C. and A.; Resources, N.A.S.; Writing—original draft, Z., N.A.S., J.D.C. and A.; Writing—review & editing, N.A.A. and A. All authors have read and agreed to the published version of the manuscript.

Funding: This work received no external fund.

Data Availability Statement: All the data is available within the manuscript.

Acknowledgments: This work was supported by the Technology Innovation Program (20018869, Development of Waste Heat and Waste Cold Recovery Bus Air-conditioning System to Reduce Heating and Cooling Load by 10%), funded by the Ministry of Trade, Industry and Energy (MOTIE, Korea).

Conflicts of Interest: The authors declare no conflict of interest.

Nomenclature

$\hat{a}(t)$	radius of the pipe
A	the injection/suction coefficient
B_0	applied magnetic field
C	dimensional nanoparticle concentration
C_0	reference nanoparticle concentration at the center
C_p	specific heat at constant pressure
C_w	nanoparticle concentration at the wall
k_1	first-order chemical reaction rate
Le	Lewis number
M	Hartmann number
Nt	thermophoresis parameter
Nb	Brownian motion parameter
Pr	Prandtl number
Q	heat source/sink parameter
r, z	dimensional cylindrical coordinates
T	dimensional temperature
T_0	reference temperature at the center
T_m	mean temperature
T_m	mean fluid temperature
T_w	temperature near the wall
u, v	velocity components along \hat{r} and \hat{z} directions respectively
v_w	injection/suction velocity
ρ_f	density of the base fluid
σ	electrical conductivity
β	thermal diffusivity
θ	dimensionless temperature
$(\rho C_p)_p$	heat capacity of the nanoparticle
ϕ	dimensionless concentration

References

- Choi, S.U.S. Enhancing Thermal Conductivity of Fluids with Nanoparticle. In *Developments and Applications of Non-Newtonian Flows*; Siginer, D.A., Wang, H.P., Eds.; FED-V.231/MDV. 66; ASME: New York, NY, USA, 1995; pp. 99–105.
- Wang, X.-Q.; Mujumdar, A.S. A review on nanofluids. Part I: Theoretical and numerical investigations. *Braz. J. Chem. Eng.* **2008**, *25*, 613–630. [[CrossRef](#)]
- Choi, S.U.S. Nanofluids: A new field of scientific research and innovative applications. *Heat Transf. Eng.* **2008**, *29*, 429–431. [[CrossRef](#)]
- Khan, W.A.; Pop, I. Boundary-layer flow of a nanofluid past a stretching sheet. *Int. J. Heat Mass Transf.* **2010**, *53*, 2477–2483. [[CrossRef](#)]
- Kumar, M.D.; Raju, C.; Sajjan, K.; El-Zahar, E.R.; Shah, N.A. Linear and quadratic convection on 3D flow with transpiration and hybrid nanoparticles. *Int. Commun. Heat Mass Transf.* **2022**, *134*, 105995. [[CrossRef](#)]
- Abderrahmane, A.; Qasem, N.A.A.; Younis, O.; Marzouki, R.; Mourad, A.; Shah, N.A.; Chung, J.D. MHD Hybrid Nanofluid Mixed Convection Heat Transfer and Entropy Generation in a 3-D Triangular Porous Cavity with Zigzag Wall and Rotating Cylinder. *Mathematics* **2022**, *10*, 769. [[CrossRef](#)]
- Shah, N.A.; Wakif, A.; El-Zahar, E.R.; Thumma, T.; Yook, S.-J. Heat transfers thermodynamic activity of a second-grade ternary nanofluid flow over a vertical plate with Atangana-Baleanu time-fractional integral. *Alex. Eng. J.* **2022**, *61*, 10045–10053. [[CrossRef](#)]
- Buongiorno, J. Convective heat transport in nanofluids. *J. Heat Transf.* **2006**, *128*, 240–250. [[CrossRef](#)]
- Roşca, N.C.; Pop, I. Unsteady boundary layer flow of a nanofluid past a moving surface in an external uniform free stream using Buongiorno's model. *Comput. Fluids* **2014**, *95*, 49–55. [[CrossRef](#)]
- Kuznetsov, A.V.; Nield, D.A. Natural convective boundarylayer flow of a nanofluid past a vertical plate. *Int. J. Therm. Sci.* **2010**, *49*, 243–247. [[CrossRef](#)]

11. Ashraf, M.Z.; Rehman, S.U.; Farid, S.; Hussein, A.K.; Ali, B.; Shah, N.A.; Weera, W. Insight into significance of bioconvection on MHD tangent hyperbolic nanofluid flow of irregular thickness across a slender elastic surface. *Mathematics* **2022**, *10*, 2592. [[CrossRef](#)]
12. Lou, Q.; Ali, B.; Rehman, S.U.; Habib, D.; Abdal, S.; Shah, N.A.; Chung, J.D. Micropolar dusty fluid: Coriolis force effects on dynamics of MHD rotating fluid when Lorentz force is significant. *Mathematics* **2022**, *10*, 2630. [[CrossRef](#)]
13. Mustafa, M.; Nawaz, M.; Hayat, T.; Alsaedi, A. MHD boundary layer flow of second grade nanofluid over a stretching sheet with convective boundary conditions. *J. Aerosp. Eng.* **2014**, *27*, 1–7. [[CrossRef](#)]
14. Alsaedi, A.; Awais, M.; Hayat, T. Effect of heat generation/absorption on stagnation point flow of nanofluid over a surface with convective boundary conditions. *Commun. Nonlinear Sci. Numer. Simul.* **2012**, *17*, 4210–4223. [[CrossRef](#)]
15. Chamkha, J.; Rashad, A.M.; Aly, A.M. Transient natural convection flow of a nanofluid over a vertical cylinder. *Meccanica* **2012**, *48*, 71–81. [[CrossRef](#)]
16. Malvandi, A.; Moshizi, S.; Soltani, E.; Ganji, D. Modified Buongiorno's model for fully developed mixed convection flow of nanofluids in a vertical annular pipe. *Comput. Fluids* **2014**, *89*, 124–132. [[CrossRef](#)]
17. Akbari, M.; Behzadmehr, A.; Shahraki, F. Fully developed mixed convection in horizontal and inclined tubes with uniform heat flux using nanofluid. *Int. J. Heat Fluid Flow* **2008**, *29*, 545–556. [[CrossRef](#)]
18. Ellahi, R. The effects of MHD and temperature dependent viscosity on the flow of non-Newtonian nanofluid in a pipe: Analytical solutions. *Appl. Math. Model.* **2013**, *37*, 1451–1467. [[CrossRef](#)]
19. Uddin, M.; Bég, O.A.; Amin, N. Hydromagnetic transport phenomena from a stretching or shrinking nonlinear nanomaterial sheet with Navier slip and convective heating: A model for bio-nano-materials processing. *J. Magn. Magn. Mater.* **2014**, *368*, 252–261. [[CrossRef](#)]
20. Xu, H.; Fan, T.; Pop, I. Analysis of mixed convection flow of a nanofluid in vertical channel with Buongiorno mathematical model. *Int. Commun. Heat Mass Transf.* **2013**, *44*, 15–22. [[CrossRef](#)]
21. Malik, M.; Naseer, M.; Nadeem, S.; Rehman, A. The boundary layer flow of Casson nanofluid over a vertical exponentially stretching cylinder. *Appl. Nanosci.* **2014**, *4*, 869–873. [[CrossRef](#)]
22. Raju, C.S.K.; Ameer, N.A.; Kiran, S.; Nehad, A.S.; Se-jin, Y.; Dinesh, M.K. Nonlinear movements of axisymmetric ternary hybrid nanofluids in a thermally radiated expanding or contracting permeable Darcy Walls with different shapes and densities: Simple linear regression. *Int. Commun. Heat Mass Transfer* **2022**, *135*, 106110. [[CrossRef](#)]
23. Ramesh, G.; Madhukesh, J.; Shah, N.A.; Yook, S.-J. Flow of hybrid CNTs past a rotating sphere subjected to thermal radiation and thermophoretic particle deposition. *Alexandria Eng. J.* **2022**, *64*, 969–997. [[CrossRef](#)]
24. Srinivas, S.; Vijayalakshmi, A.; Ramamohan, T.; Reddy, A.S. Hydromagnetic flow of a nanofluid in a porous channel with expanding or contracting walls. *J. Porous Media* **2014**, *17*, 953–967. [[CrossRef](#)]
25. Hedayati, F.; Domairry, G. Effects of nanoparticle migration and asymmetric heating on mixed convection of TiO₂-H₂O nanofluid inside a vertical micro channel. *Powder Technol.* **2015**, *272*, 250–259. [[CrossRef](#)]
26. Malvandi, A.; Safaei, M.; Kaffash, M.; Ganji, D. MHD mixed convection in a vertical annulus filled with Al₂O₃-water nanofluid considering nanoparticle migration. *J. Magn. Magn. Mater.* **2015**, *382*, 296–306. [[CrossRef](#)]
27. Vajravelu, K.; Prasad, K.; Rao, N.P. Diffusion of a chemically reactive species of a power-law fluid past a stretching surface. *Comput. Math. Appl.* **2011**, *62*, 93–108. [[CrossRef](#)]
28. Na, W.; Tlili, I.; Siddique, I. Maxwell fluid flow between vertical plates with damped shear and thermal flux: Free convection. *Chin. J. Phys.* **2020**, *65*, 367–376. [[CrossRef](#)]
29. Mahsud, Y.; Vieru, D. Influence of time-fractional derivatives on the boundary layer flow of Maxwell fluids. *Chin. J. Phys.* **2017**, *55*, 1340–1351. [[CrossRef](#)]
30. Nadeem, S.; Akbar, N. Influence of heat and chemical reactions on Walter's B fluid model for blood flow through a tapered artery. *J. Taiwan Inst. Chem. Eng.* **2011**, *42*, 67–75. [[CrossRef](#)]
31. Hayat, T.; Abbas, Z. Channel flow of a Maxwell fluid with chemical reaction. *Z. Angew. Math. Phys.* **2008**, *59*, 124–144. [[CrossRef](#)]
32. Abdul-Kahar, R.; Kandasamy, R. Muhaimin, Scaling group transformation for boundary-layer flow of a nanofluid past a porous vertical stretching surface in the presence of chemical reaction with heat radiation. *Comput. Fluids* **2011**, *52*, 15–21. [[CrossRef](#)]
33. Kameswaran, P.; Shaw, S.; Sibanda, P.; Murthy, P. Homogeneous–heterogeneous reactions in a nanofluid due to a porous stretching sheet. *Int. J. Heat Mass Transf.* **2013**, *57*, 465–472. [[CrossRef](#)]
34. Uddin, M.; Khan, W.; Ismail, A. Lie group analysis and numerical solutions for magneto convective slip flow along a moving chemically reacting radiating plate in porous media with variable mass diffusivity. *Heat Transf.-Asian Res.* **2014**, *45*, 239–263. [[CrossRef](#)]
35. Rashidi, M.; Momoniat, E.; Ferdows, M.; Basiriparsa, A. Lie group solution for free convective flow of a nanofluid past a chemically reacting horizontal plate in porous media. *Math. Probl. Eng.* **2014**, *2014*, 1–21. [[CrossRef](#)]
36. Srinivas, S.; Reddy, A.S.; Ramamohan, T. Mass transfer effects on viscous flow in an expanding or contracting porous pipe with chemical reaction. *Heat Transf.-Asian Res.* **2015**, *44*, 552–567. [[CrossRef](#)]
37. Uddin, M.; Bég, O.; Aziz, A.; Ismail, A. Group analysis of free convection flow of a magnetic nanofluid with chemical reaction. *Math. Probl. Eng.* **2015**, *2015*, 1–11. [[CrossRef](#)]
38. Uchida, S.; Aoki, H. Unsteady flows in a semi-infinite contracting or expanding pipe. *J. Fluid Mech.* **1977**, *82*, 371–387. [[CrossRef](#)]

39. Goto, M.; Uchida, S. Unsteady flows in a semi-infinite contracting or expanding pipe with a porous wall. *Theor. Appl. Mech.* **1991**, *40*, 161–172.
40. Majdalani, J.; Zhou, C. Moderate-to-large injection and suction driven channel flows with expanding or contracting walls. *Z. Angew. Math. Mech.* **2003**, *83*, 181–196. [[CrossRef](#)]
41. Shah, N.A.; Zafar, A.A.; Akhtar, S. General solution for MHD-free convection flow over a vertical plate with ramped wall temperature and chemical reaction. *Arab. J. Math.* **2018**, *7*, 49–60. [[CrossRef](#)]
42. Majdalani, J.; Flandro, G.L. The oscillatory pipe flow with arbitrary injection. *Proc. R. Soc. Lond. A* **2002**, *458*, 1621–1651. [[CrossRef](#)]
43. Khan, I.; Shah, N.A.; Dennis, L.C.C. A scientific report on heat transfer analysis in mixed convection flow of Maxwell fluid over an oscillating vertical plate. *Sci. Rep.* **2017**, *7*, srep40147. [[CrossRef](#)]
44. Terrill, R.; Thomas, P. Spiral flow in a porous pipe. *Phys. Fluids* **1973**, *16*, 356–359. [[CrossRef](#)]
45. Sajjan, K.; Ahammad, N.; Raju, C.; Kumar, M.; Weera, W. Nonlinear Boussinesq and Rosseland approximations on 3D flow in an interruption of Ternary nanoparticles with various shapes of densities and conductivity properties. *AIMS Math.* **2022**, *7*, 18416–18449. [[CrossRef](#)]
46. Boutros, Y.; Abd-El-Malek, M.; Badran, N.; Hassan, H. Lie-group method for unsteady flows in a semi-infinite expanding or contracting pipe with injection or suction through a porous wall. *J. Comput. Appl. Math.* **2006**, *197*, 465–494. [[CrossRef](#)]
47. Zeeshan. Heat enhancement analysis of Maxwell fluid containing molybdenum disulfide and graphene nanoparticles in engine oil base fluid with isothermal wall temperature conditions. *Waves Random Complex Media* **2023**, 1–15. [[CrossRef](#)]
48. Zeeshan; Ahammad, N.A.; Rasheed, H.; El-Deeb, A.A.; Almarri, B.; Shah, N.A. Numerical Intuition of Activation Energy in Transient Micropolar Nanofluid Flow Configured by an Exponentially Extended Plat Surface with Thermal Radiation Effects. *Mathematics* **2022**, *10*, 4046. [[CrossRef](#)]
49. Zeeshan; Attaullah; Ahammad, N.A.; Shah, N.A.; Chung, J.D. A Numerical Framework for Entropy Generation Using Second-Order Nanofluid Thin Film Flow over an Expanding Sheet: Error Estimation and Stability Analysis. *Mathematics* **2023**, *11*, 1078. [[CrossRef](#)]
50. Zeeshan; Ahammad, N.A.; Shah, N.A.; Chung, J.D.; Attaullah; Rasheed, H.U. Analysis of Error and Stability of Nanofluid over Horizontal Channel with Heat/Mass Transfer and Nonlinear Thermal Conductivity. *Mathematics* **2023**, *11*, 690. [[CrossRef](#)]
51. Raza, J.; Mebarek-Oudina, F.; Lund, L. The flow of magnetised convective Casson liquid via a porous channel with shrinking and stationary walls. *Pramana* **2022**, *96*, 229. [[CrossRef](#)]
52. Khan, U.; Mebarek-Oudina, F.; Zaib, A.; Ishak, A.; Abu Bakar, S.; Sherif, E.-S.M.; Baleanu, D. An exact solution of a Casson fluid flow induced by dust particles with hybrid nanofluid over a stretching sheet subject to Lorentz forces. *Wave Random Complex* **2022**, *2022*, 1–14. [[CrossRef](#)]
53. Chabani, I.; Mebarek-Oudina, F.; Vaidya, H.; Ismail, A.I. Numerical analysis of magnetic hybrid nano-fluid natural convective flow in an adjusted porous trapezoidal enclosure. *J. Magn. Magn. Mater.* **2022**, *564*, 170142. [[CrossRef](#)]
54. Liao, S.J. *Beyond Perturbation: Introduction to Homotopy Analysis Method*; CRC Press; Chapman and Hall: Boca Raton, FL, USA, 2003.

Disclaimer/Publisher's Note: The statements, opinions and data contained in all publications are solely those of the individual author(s) and contributor(s) and not of MDPI and/or the editor(s). MDPI and/or the editor(s) disclaim responsibility for any injury to people or property resulting from any ideas, methods, instructions or products referred to in the content.